

Ultra-sensitive curvature sensor based on liquid crystal-infiltrated fiber interferometer

Meng-Zhu Zhang¹, Yu-Ming Ge¹, Shin-Tson Wu² and Shug-June Hwang^{1,2}

¹ Department of Electro-Optical Engineering, National United University, Maio-Li, 360, Taiwan

² College of Optics and Photonics, University of Central Florida, Orlando, FL 32816, USA

E-mail: june@nuu.edu.tw

Received 14 May 2016, revised 22 August 2016

Accepted for publication 20 October 2016

Published 22 November 2016



CrossMark

Abstract

All-fiber curvature sensors based on a liquid crystal-filled fiber Mach–Zehnder interferometer (LCF-MZI) are proposed and experimentally demonstrated for high performance measurements of very small curvatures from 0 to 0.0667 m^{-1} , which is usually hard to be precisely monitored by well-known methods. Such a curvature sensor can be easily fabricated by splicing a section of an LC-filled hollow core fiber between two single mode fibers. Our experimental results show that the maximum curvature sensitivity of the proposed sensor is -724.3 nm/m^{-1} for a wavelength shift and 632 dB/m^{-1} for peak intensity. These results are at least 10 times better than those of previously reported fiber interferometer sensors.

Keywords: optical fiber sensor, liquid crystal fiber, Mach–Zehnder interferometer, curvature sensor, hollow optical fiber

(Some figures may appear in colour only in the online journal)

1. Introduction

All-fiber sensors have been extensively investigated for various sensing applications because of their unique advantages in compactness, relatively simple fabrication process, high sensitivity, high resolution, and immunity to electromagnetic interference. It is a useful device for monitoring the external disturbance including pressure, displacement, temperature, external refractive index, and curvature [1–6]. Among these applications, curvature sensing is particularly important in smart structures, artificial limbs, aerospace industry, robot arms, and medical treatment. Several high performance fiber-optic curvature sensors [5–14] have been demonstrated. For example, Gong *et al* [6] reported a curvature sensor using a single-mode–multimode–single-mode fiber structure with a maximum sensitivity of wavelength-curvature 10.38 nm/m^{-1} in the large curvature range ($>0.25\text{ m}^{-1}$). Delgado's group [7] applied a seven-core fiber to turn a super-mode interferometer into a curvature sensor with a sensitivity of $\sim 3\text{ nm/m}^{-1}$ in the curvature range of 2.2 m^{-1} to 5 m^{-1} . Guzman-Sepulveda *et al* [8] demonstrated a curvature sensor based on a two-core fiber with high sensitivity of -137.87 nm/m^{-1} at the curvature regime from 0 to 0.27 m^{-1} , and Gong *et al* [8] manufactured a curvature sensor based on a two peanut-shaped structure

modal interferometer with the sensitivity of -21.87 nm/m^{-1} in the range of 2.5 m^{-1} to 4.2 m^{-1} .

Among these reported photonic devices, the most attractive fiber sensor configuration is based on the Mach–Zehnder interferometer (MZI) [5–13]. To achieve an in-fiber MZI, a relative phase difference of two beams originated from the same laser light is required; this can be realized by allowing the two beams to travel in different paths. Based on the principle of the mode interference, the optic spectrum of the fiber interferometer can sensitively vary with respect to perturbation from external parameters. By properly choosing the measured wavelength shifts or intensity changes, the external field measurement with high sensitivity can be obtained. However, these high sensitivity fiber-optic sensors necessitate complex processes or expensive fabrication apparatus and are limited to monitoring a relatively large curvature, i.e. small curvature radius. When the curvature is smaller than 0.1 m^{-1} , these sensors do not work well, especially for mechanical deformation of artificial limbs, robots, health, and medical materials.

To overcome this bottleneck, we demonstrate a new liquid crystal-infiltrated fiber Mach–Zehnder interferometer (LCF-MZI) sensor, which is realized by splicing a section of LC-filled hollow optical fiber (HOF) between two single mode fibers (SMFs) [15]. We have demonstrated that the

transmission spectrum of such a MZI fiber can be governed by thermal-optic characteristics of LC materials (i.e. the temperature gradient of the LC refractive index $\partial(\delta n_{\text{eff}}^{\text{LC}})/\partial T$), because the refractive index and directors of LCs can be altered by temperature. Therefore this proposed LCF-MZI has been applied to be a thermal sensor with very high sensitivity. Moreover, the orientation of liquid crystal molecules (LCs) is highly sensitive to external fields, e.g. mechanical, electric field or magnetic fields. An external mechanical disturbance such as bending will significantly modulate the reorientation of the LC director and then alter the effective refractive index of an LC fiber. This bending-induced effective refractive index variation of LCF will notably alter the optical properties of MZI and provide the resultant mode interference effect with a sharp spectral change for accurately determining the curvature. Our experimental results show that this novel yet simple LCF-MZI fiber sensor is capable of accurately measuring a small curvature less than 0.067 m^{-1} with an ultrahigh sensitivity. Compared to previously reported devices, our sensor shows significant advantages in sensitivity and detectable ranges.

2. Operational principle

We have developed a novel and simple technique to achieve an all-fiber MZI based on LC-filled HOF [15]. Figure 1 schematically illustrates the structure and operating principle of the proposed LCF-MZI, which is realized by arc-fusing one LC-infiltrated HOF with length L spliced between two standard single-mode lead-in/lead-out fibers, which act as the input and output ports for light. The fundamental mode guided through the SMF core on the left-hand side is divided into two main portions by the first abrupt tapered section as it enters the HOF; one directly passes through the air core and the LC-infiltrated section of HOF, while the other passes along the core-cladding boundary in a cladding mode. The generated core mode (I_{co}) and cladding mode (I_{clad}) propagate along the HOF with different optic paths and are recombined as they pass through the second tapered section. As a result, the interference occurs at the second single mode fiber and the phase difference Φ between the cladding mode and the core mode of a MZI fiber device can be expressed as:

$$\Phi = \frac{2\pi \Delta n_{\text{eff}} L}{\lambda} \quad (1)$$

where L is the length of HOF, Δn_{eff} is the difference of the effective refractive indices between the core mode and the cladding mode, and λ is the operating wavelength. The accumulated optical path difference over the HOF-based MZI is $\Delta n_{\text{eff}} L = (n_{\text{eff}}^{\text{co}} - n_{\text{eff}}^{\text{clad}}) L = \delta n_{\text{eff}}^{\text{LC}} L_{\text{LC}} + \delta n_{\text{eff}}^{\text{air}} (L - L_{\text{LC}})$, where L_{LC} is the length of the LC section in HOF, $\delta n_{\text{eff}}^{\text{LC}}$ and $\delta n_{\text{eff}}^{\text{air}}$ represent the difference of the effective refractive indices between the core mode and the cladding mode for the LC segment and air core, respectively. Due to the interference effect between different pairs of modes, the transmitted intensity reaches its minimum value, called transmission notch, when the phase difference between two modes is equal to

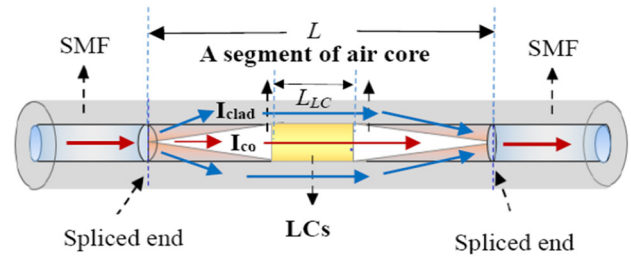


Figure 1. Schematic diagram of the LCF-MZI fiber sensor, in which the tapering structure was formed by arc-fusing at both of the spliced ends.

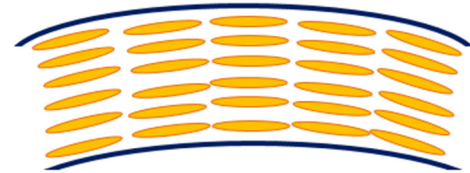


Figure 2. The alignment of LCs in the hollow core fiber under bending situation.

an odd multiple of π . Thus the notch wavelength λ_m of the interference signal reaching its minimum can be expressed as $\lambda_m = 2\Delta n_{\text{eff}} L / (2m + 1)$. Here m is the interference order.

To investigate the curvature sensing capability of LCF-based MZI, we measured the spectral shift induced by bending. Because the orientation of LC molecules inside HOF is highly sensitive to the external field, a small external mechanical disturbance will cause a large fringe interference shift. When LCF-MZI is bent, not only does the effective refractive index of the cladding layer change, but also the reorientation of LC molecules inside the core of HOF occurs as shown in figure 2. The bent-shape reorientation of LCs will make light deflected away from the guiding direction [16–18] and modulate the effective refractive index of the core mode. As a result, the curvature dramatically changes the optical properties of the proposed MZI. In addition, the refractive index profile of the fiber core becomes asymmetric due to elasto-optic and geometrical changes in the refractive index. The bending-induced differential phase retardation between the propagating core and cladding modes is notably influenced by the curvature radius, which in turn causes the transmission spectrum to shift in wavelength and then the minimum intensity of the interference notches changes. Here, as the device is kept straight, the transmission spectra have notch wavelength values. This initial value can be considered as the zero bending condition. Tracing the wavelength shift or the intensity variation of the interference notches in the transmission spectrum as the sensor device is bent would allow us to precisely and reliably measure the bending radius.

3. Experimental

For fabricating all-fiber MZI based on liquid crystal-filled fiber, we used a hollow optical fiber TSP010150 (Polymicro), in which the inner and outer radii of the HOF were measured to be $8.5 \mu\text{m}$ and $125 \mu\text{m}$, respectively. First, we filled an LC



Figure 3. Optical microscope image of (a) the tapering structure formed by arc-fusing at both of the spliced ends, and (b) the LC-filled fiber between crossed polarizers.

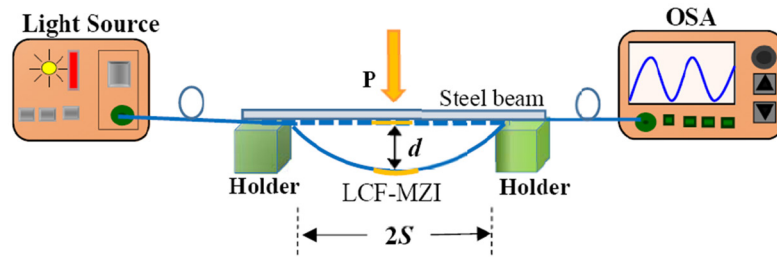


Figure 4. Schematic diagram of the experimental setup for measuring the curvature of the LC-MZI fiber.

material (RDP-98995, DIC Corp.) into the hollow fiber for an LC length of $L_{LC} = 620 \mu\text{m}$ by capillary flow. The refractive indices of RDP-98995 are $n_o = 1.484$ and $n_e = 1.575$ at $\lambda = 589 \text{ nm}$ and $25 \text{ }^\circ\text{C}$. Next, we assembled the two end faces of the LC-filled HOF with two SMFs using a commercial fusion splicer. During this splicing process, the air hole at both splicing ends of the HOF collapsed to form abrupt tapering structures near the two spliced joints as shown in figure 3(a). The tapered structure functions as a beam splitter and combiner; the former excites several cladding modes at the front end and the latter recombines the core-mode light and the cladding-mode light into the second SMF to achieve the interference signals. To obtain high coupling efficiency at both two jointed ends, an optimum abrupt tapering structure should be achieved by adjusting the arc-splicing condition. Besides, the electric arc-discharge inherently generates significant heat on the LC-filled fiber and then burnout the LC material during the splicing procedure. To keep away from the scorch of an LC material caused by splicing-induced overheat, some space of the HCF near the two jointed ends should be left. In this work, the total length of the air core at the front and rear ends of HOF is fixed at $L_{\text{air}} = L - L_{LC} \sim 7 \text{ mm}$. Due to capillary force, the LC alignment inside the HOF is parallel to the fiber axis as depicted in figure 3(b), making the incoming laser beam mainly experience the ordinary refractive index in all polarized direction. As a result, the optical properties of LCF-MZI are polarization-independent.

The experimental setup to measure the curvature using our proposed fiber sensor is shown in figure 4, which is similar to that used in [6]. The LCF-MZI was placed just in the middle distance between the two holders. The separation ($2S$) between the two holders was fixed at 60 cm . Both fiber ends were not fixed and the fiber under the metal beam was flexible. In this arrangement, the LCF-MZI structure can bend freely and synchronously with the metal beam. In addition, the MZI fiber is symmetrically bent along with the lead-in and lead-out SMFs.

To tune the curvature of the MZI fiber (ρ) with that of the metal beam, we adjusted the bending displacement (d) by carefully pressing the center of the MZI fiber structure. Then the fiber curvature could be easily determined by using the formula: $\rho = 2d/(d^2 + S^2)$, with S the half separation between the edges of the two holders. For investigating how the LC-MZI fiber sensor responds to bending, we connected the SMF input port of the interferometer to a broadband light source (BLSS101B-028002A; GIP Tech. Corp.), and the SMF output port to an optical spectrum analyzer (OSA; Anritsu MS9740A) with the wavelength band from 1250 nm to 1650 nm to record the transmission spectrum. To design the bending sensor, an initial phase difference should be first obtained for the fiber sensor without any bending. In this work, we control the bending displacement of MZI from 0 to 3 mm to study the bending effect on the transmission band of LCF-MZI.

4. Results and discussion

The transmitted spectra of the LC-MZI fiber sensor under different bending curvatures were measured and shown in figure 5. The spectra obtained with different curvatures are identified by the various values of bending displacement, d , from which the corresponding curvature can be determined. Without any bending displacement (i.e. $d = 0$), strong interferences are observed and interference fringes have a dynamic range over 22 dB , which is adequate for most sensing applications. The background loss of the device is $\sim 8 \text{ dB}$, which is mainly caused by the two abrupt tapers. Although the tapering structure of LCF-MZI, such as tapering angle and length, noticeably influences the optical power distributed between the core and cladding layers from the input SMF; the geometry of the tapered sections only makes an impact on the dynamic range of the interference fringes, it can not affect the notch wavelength λ_m of the interference signal which is governed

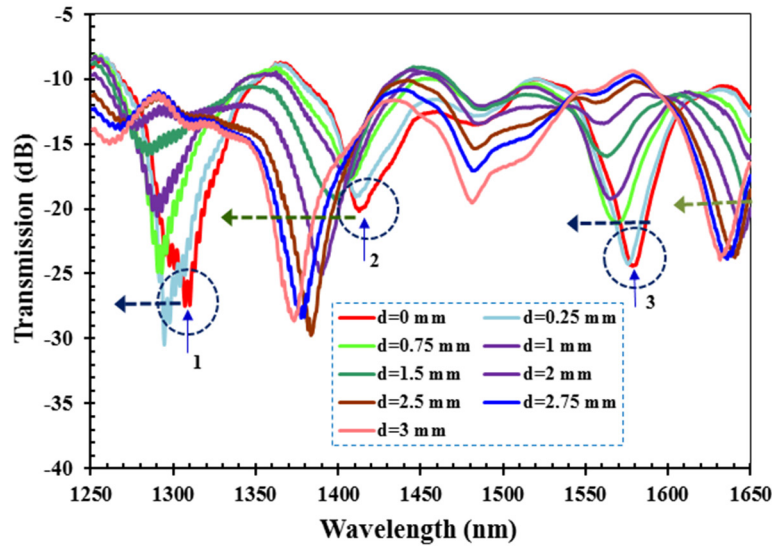


Figure 5. Measured transmission spectra of the LC-MZI fiber device under different bending curvatures.

by the phase differences between core and cladding modes. In this work, by adjusting the fusion-splicing condition, an optimum abrupt tapering structure was successfully achieved near two spliced joints to obtain high coupling efficiency at both jointed ends and very deep notches in the transmission spectrum.

According to our experimental results, we found three main corresponding transmission notches being particularly deep in the spectral range of 1250–1650 nm. The wavelengths at which these notches occur are highly sensitive to the physical external disturbance, especially for mechanical bending. From figure 5, the wavelength and the transmission minima of these three notches change gradually with increasing curvature. All of the three interference patterns experience a bending-induced blue-shift; however, the orders of modes interfering with each other do not change as the applied curvature changes. In addition, different transmission notches have different curvature characteristics. For example, the transmission minima of the third notch ~1580 nm progressively decreases with the curvature and finally nearly disappears and at the same time, a new transmission notch gradually appears and becomes deeper in the spectra around 1480 nm as the applied curvature increases; but the transmission minima of the second notch became deeper for a larger bending displacement, which was different from that of the 3rd notch. Because the purpose of this work is mainly concerned on proposing a simple and novel LCF-MZI, as well as exploring the notch wavelength of MZI in response to a mechanical field. The theoretical analysis for the distributed modes was not performed here. Theoretically, the optical field distributed in the core and cladding layers and the interference properties of LCF-MZI is extremely dependent on the refractive index difference between core and cladding layer, core diameter, tapering geometry, the LC length, and incident light wavelength. The effective refractive index of fiber core, however, is controlled by the alignment and refractive index of LCs which is critically influenced by the inner surface treatment of HOF, LC material properties (such as the elastic constant, viscosity, etc), LC-infiltrated force and so on.

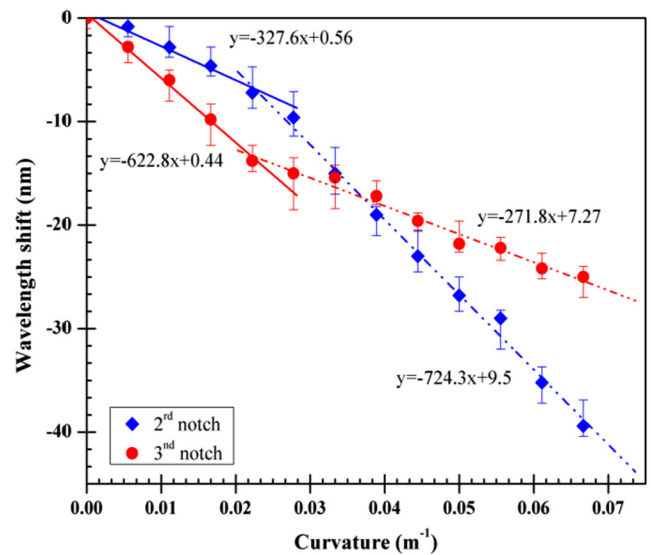


Figure 6. Transmission notch wavelength shift of the MZI fiber as a function of curvature.

Hence the theoretical analysis of the propagating modes in LC-MZI is much more complicated. To significantly improve the proposed operational principle of the sensor, a detailed analysis will be performed in the future.

Based on the above measured spectra of the LC-MZI fiber, bending could be certainly identified by the notch wavelength shift and minimum intensity of the spectral interference features. To investigate the bending-induced notch spectra variation for different curvature conditions, we only analyze the bending-induced notch wavelength shift and minimum intensity for the 2nd and 3rd notches. Figure 6 shows the measured transmission notch wavelength shift as the curvature increases. In general, the relationship between wavelength shift and curvature is not linear, and blue shift of the notch wavelength gradually increases with the curvature for both 2nd and 3rd notches, λ_2 and λ_3 . More amazingly, our LC-MZI fiber is extremely sensitive to curvature changes;

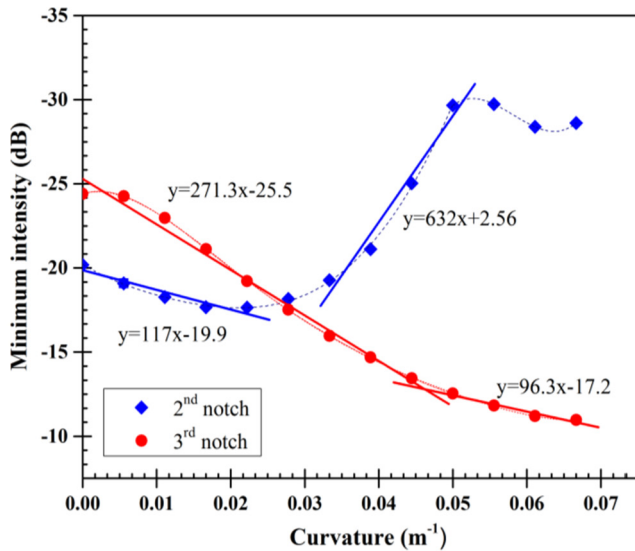


Figure 7. Minimum transmission of the LC-MZI fiber structure as a function of curvature.

a tiny curvature of 0.0667 m^{-1} (i.e. $d = 3 \text{ mm}$) can cause a significant blue shift of 39.4 nm and 25 nm for the 2nd and 3rd notches, respectively. To determine the wavelength-curvature sensitivity of these two notches, the linear fittings method was applied; this is a common method as reported in [6–7, 13–14]. From figure 6, the sensor's response can be roughly divided into two linear regions: $0 < \rho < 0.0222 \text{ m}^{-1}$ and $0.0222 < \rho < 0.0667 \text{ m}^{-1}$. The coupling coefficient between the core and cladding modes is changed as the fiber is bent. When the fiber was under the curvature around 0.022 mm^{-1} , an abrupt change of wavelength shift occurred owing to a high variation of the coupling coefficient being induced. The minimum sensitivity is still larger than -271 nm/m^{-1} as indicated in the 3rd notch. Especially, the second notch exhibits an ultrahigh sensitivity of -724.3 nm/m^{-1} in the curvature range $0.0222 < \rho < 0.0667 \text{ m}^{-1}$, while the third notch also exhibits a great sensitivity of -622.8 nm/m^{-1} in the curvature range of $0 < \rho < 0.0222 \text{ m}^{-1}$. According to the experimental results, the measured bending sensitivity of the proposed LC-MZI fiber is at least $10 \times$ higher than those previously reported [6–12] in the ultra-small curvature situation $0 < \rho < 0.0667 \text{ m}^{-1}$. Besides, it is worth mentioning that the minimum curvature variation the proposed sensor can detect is $0.22 \times 10^{-3} \text{ m}^{-1}$.

Figure 7 shows the transmission minima of the 2nd and 3rd notches as a function of curvature change. The behaviors of the 2nd and the 3rd notches are quite different. For the 3rd notch, the transmission minimum gradually decreases with the curvature. But for the 2nd notch, the tendency could increase or decrease depending on the curvature range. Through linear fittings, a sensitivity of 271.3 dB/m^{-1} and 96.3 dB/m^{-1} for the 2nd notch is obtained in the $0 < \rho < 0.05 \text{ m}^{-1}$ and $0.05 < \rho < 0.067$ regions, respectively. For the 3rd interference notch, the obtained sensitivity is 117 dB/m^{-1} at $0 < \rho < 0.022 \text{ m}^{-1}$ and 632 dB/m^{-1} at $0.033 < \rho < 0.0556 \text{ m}^{-1}$. These results indicate that our proposed LC-MZI fiber sensor exhibits an excellent sensitivity in the small curvature range, which is tough to compete by other kinds of

fiber-optic curvature sensors. Both curvature sensitivity and detectable curvature range are at least 10 times better than those previously reported. In addition, because the alignment of LC molecules in the hollow core is highly sensitive to the bending curvature, the sensitivity of the attenuation notch wavelength with respect to the curvature change is mainly attributed to the length of LCF-MZI and curvature-induced effective refractive index variation. Therefore we observed that the repeatability and stability of the experimental data with respect to fluctuations in taper geometry during fabrication is very high.

The effective refractive index of the LC-infiltrated fiber strongly depends on the molecular alignment and birefringence of the employed LC material. The former is sensitive to bending, while the latter is dependent on the ambient temperature [19]. To compare the contributions of these two effects, we analyzed the temperature-induced wavelength peak shift. Our measured wavelength-temperature sensitivity of the proposed LC-MZI fiber was about $0.7 \text{ nm } ^\circ\text{C}^{-1}$ in the range of $25\text{--}60 \text{ }^\circ\text{C}$. Thus, the wavelength shift induced by the ambient temperature variation is much smaller than that induced by the curvature. Therefore, as long as the ambient temperature is kept constant or isolated by using a temperature-insensitive material, the temperature effect of our curvature sensor can be neglected. Further research for simultaneously monitoring the temperature and curvature by our LC MZI fiber is in progress. Due to its high sensitivity, wide detectable range, and simple fabrication process, our proposed LC-MZI fiber is an excellent candidate for a wavelength dependent curvature sensor, which is potentially useful in a broad range of MEMS structure, smart material, and medical instruments including prosthetic limbs, robots, and so on. Additionally, in order to protect the splicing joint of LCF-MZI, a heat shrink tubing, silicone gel and/or mechanical crimp protector can be applied to make the proposed compact MZI fiber suitable as a sensor to detect bending, strain, and refractive index of an object.

5. Conclusion

We demonstrated a novel yet simple, cost-effective, and highly sensitive fiber-optic curvature sensor based on Mach-Zehnder's interferometer by splicing a section of liquid crystal-filled hollow-optic fiber between two SMFs. The curvature sensing characteristics, such as bending-induced shifts of wavelength and minimum intensity of the spectrum, are experimentally investigated. The proposed sensor utilizes two unique features: the core/cladding mode interference and liquid crystal which is highly sensitive to an external disturbance. Thus, our sensor is very sensitive to curvature changes and can be applied to monitor objects with very small curvatures. In our concept proof experiments, we achieved a maximum curvature sensitivity of -724.3 nm/m^{-1} and 632 dB/m^{-1} for a curvature range from 0.02 to 0.0667 m^{-1} and 0.3 to 0.5 m^{-1} , respectively. Compared to the previously reported fiber curvature sensors, our LC-infiltrated MZI fiber sensor exhibits at least 10 times higher sensitivity.

Acknowledgments

The authors are indebted to the Ministry of Science and Technology of Taiwan for financial support under contract MOST 103-2221-E-239-003, Giantplus Tech. Corp. for providing the liquid crystal material, and technical assistance from Prof Nan-Kung Chen of the National United University, Taiwan.

References

- [1] Urban F, Kadlec J, Vlach R and Kuchta R 2010 Design of a pressure sensor based on optical fiber Bragg grating lateral deformation *Sensors* **10** 11212–25
- [2] Li G, Li Y, Yang K and Liu M 2014 Fiber-optic displacement sensor based on the DBR fiber laser *Photonic Sensors* **4** 43–7
- [3] Hu T Y, Wang Y, Liao C R and Wang D N 2012 Miniaturized fiber in-line Mach–Zehnder interferometer based on inner air cavity for high-temperature sensing *Opt. Lett.* **37** 5082–4
- [4] Yang J, Jiang L, Wang S, Li B, Wang M, Xiao H, Lu Y and Tsai H 2011 High sensitivity of taper-based Mach–Zehnder interferometer embedded in a thinned optical fiber for refractive index sensing *App. Opt.* **50** 5503–7
- [5] Monzon-Hernandez D, Martinez-Rios A, Torres-Gomez I and Salceda-Delgado G 2011 Compact optical fiber curvature sensor based on concatenating two tapers *Opt. Lett.* **36** 4380–2
- [6] Gong Y, Zhao T, Rao Y-J and Wu Y 2011 All-fiber curvature sensor based on multimode interference *IEEE Photon. Tech. Lett.* **23** 679–81
- [7] S-Delgado G, Newkirk A V, A-Lopez J E, M-Rios A, Schülzgen A and Correa R A 2015 Compact fiber-optic curvature sensor based on super-mode interference in a seven-core fiber *Opt. Lett.* **40** 1468–71
- [8] Guzman-Sepulveda J R, Fuentes-Fuentes M A, Sánchez-Mondragón J J and May-Arrijoja D A 2014 High-sensitivity curvature sensor based on two-core fiber *Latin America Optics and Photonics Conf.* Paper# LTh2C.5
- [9] Gong H, Yang X, Ni K, Zhao C-L and Don X 2014 An optical fiber curvature sensor based on two peanut-shape structures modal interferometer *IEEE Photon. Tech. Lett.* **26** 22–4
- [10] Yin G L, Lou S Q, Lu W L and Wang X 2014 A high-sensitive fiber curvature sensor using twin core fiber-based filter *Appl. Phys. B* **115** 99–104
- [11] Gong H P, Song H F, Li X R, Wang J F and Dong X Y 2013 An optical fiber curvature sensor based on photonic crystal fiber modal interferometer *Sensors Actuators A* **195** 139–41
- [12] Guan S and Yu Q 2014 Index-insensitive curvature sensor based on holey fiber modal interferometer *Microw. Opt. Technol. Lett.* **56** 1709–11
- [13] Shin W, Lee Y L, Yu B-A, Noh Y-C and Ahn T J 2010 Highly sensitive strain and bending sensor based on in-line fiber Mach–Zehnder interferometer in solid core large mode area photonic crystal fiber *Opt. Commun.* **283** 2097–101
- [14] Martins H, Marques M B, Jorge P, Cordeiro C M B and Frazaó O 2012 Intensity curvature sensor based on photonic crystal fiber with three coupled cores *Opt. Commun.* **285** 5128–31
- [15] Ho B-Y, Su H-P, Tseng Y-P, Wu S-T and Hwang S-J 2015 Temperature effects of Mach–Zehnder Interferometer using a liquid crystal-filled fiber *Opt. Express* **23** 33588–96
- [16] Hays M R, Wang H and Oates W S 2012 Nonlinear bending mechanics of hygroscopic liquid crystal polymer networks *J. Appl. Mech.* **79** 021009–18
- [17] Yang Y, Chen G, Martinez-Miranda L J, Yu H, Liu K and Nie Z 2016 Synthesis and liquid-crystal behavior of bent colloidal silica rods *J. Am. Chem. Soc.* **138** 68 – 71
- [18] Jin L, Lin Y and Huo Y 2011 A large deflection light-induced bending model for liquid crystal elastomers under uniform or non-uniform illumination *Int. J. Solids Struct.* **48** 3232–42
- [19] Li J, Gauza S and Wu S-T 2004 Temperature effect on liquid crystal refractive indices *J. Appl. Phys.* **96** 19–24